



OPEN

The effect of fluorescent nanodiamonds on neuronal survival and morphogenesis

SUBJECT AREAS:

CELL-PARTICLE
INTERACTIONS

NANOPARTICLES

Yung-An Huang^{1,2*}, Chun-Wei Kao^{1,3*}, Kuang-Kai Liu¹, Hou-Syun Huang^{1,4}, Ming-Han Chiang³,
Ching-Ren Soo³, Huan-Cheng Chang⁴, Tzai-Wen Chiu^{1,3}, Jui-I Chao^{1,3} & Eric Hwang^{1,2,3}Received
6 August 2014Accepted
13 October 2014Published
5 November 2014

Correspondence and requests for materials should be addressed to T.-W.C. (twchiu@g2.nctu.edu.tw); J.-I.C. (jjchao@faculty.nctu.edu.tw) or E.H. (hwangeric@mail.nctu.edu.tw)

* These authors contributed equally to this work.

¹Department of Biological Science and Technology, National Chiao Tung University, Hsinchu 30068, Taiwan, ²Institute of Bioinformatics and Systems Biology, National Chiao Tung University, Hsinchu 30068, Taiwan, ³Institute of Molecular Medicine and Bioengineering, National Chiao Tung University, Hsinchu 30068, Taiwan, ⁴Institute of Atomic and Molecular Sciences, Academia Sinica, Taipei 10672, Taiwan.

Nanodiamond (ND) has emerged as a promising carbon nanomaterial for therapeutic applications. In previous studies, ND has been reported to have outstanding biocompatibility and high uptake rate in various cell types. ND containing nitrogen-vacancy centers exhibit fluorescence property is called fluorescent nanodiamond (FND), and has been applied for bio-labeling agent. However, the influence and application of FND on the nervous system remain elusive. In order to study the compatibility of FND on the nervous system, neurons treated with FNDs *in vitro* and *in vivo* were examined. FND did not induce cytotoxicity in primary neurons from either central (CNS) or peripheral nervous system (PNS); neither did intracranial injection of FND affect animal behavior. The neuronal uptake of FNDs was confirmed using flow cytometry and confocal microscopy. However, FND caused a concentration-dependent decrease in neurite length in both CNS and PNS neurons. Time-lapse live cell imaging showed that the reduction of neurite length was due to the spatial hindrance of FND on advancing axonal growth cone. These findings demonstrate that FNDs exhibit low neuronal toxicity but interfere with neuronal morphogenesis, and should be taken into consideration when applications involve actively growing neurites (e.g. nerve regeneration).

Nanodiamond (ND), a carbon derivative nanomaterial has become a promising candidate for biomedical applications^{1–9}. NDs have been evaluated as a new class of nanocarrier for chemotherapeutic drugs by covalent or non-covalent linkages^{4,8}. Moreover, ND containing nitrogen-vacancy centers can emit fluorescence property without photobleaching that is called fluorescent nanodiamond (FND), which has been applied for bio-labeling agent^{10,11}. Although FNDs did not induce significant toxicity in various cellular and animal systems^{12,13}, the effects of FNDs on the nervous system are still unclear.

The excellent biocompatibility of nanodiamond (ND) in various biological systems has made it a promising carbon nanomaterial for therapeutic applications, especially in cancer therapy. It has recently been demonstrated that doxorubicin-complexed ND markedly reduced the brain tumor via convection-enhanced intracranial delivery¹⁴. This result opens up the possibility of using ND to treat nervous system-related diseases and injuries. Previous researches have demonstrated the low cytotoxicity of ND in primary neurons or neurons derived from embryonal carcinoma cells^{15–17}. Thalhammer *et al.* first demonstrated that culturing mouse hippocampal neurons on ND monolayer did not affect the neuronal attachment, neurite outgrowth, or cell-autonomous neuronal excitability compared to the traditional ECM coating¹⁵. The same group recently showed that the size and curvature of the NDs exhibited a significant correlation with neurite extension, the smaller the nanodiamond the longer the neurites extend¹⁶. Other diamond or diamond-like carbon surfaces have also been tested and exhibited excellent biocompatibility with neurons^{18,19}. These researches suggested ND as a potential material for drug delivery in the nervous system. However, none of the experiments mentioned above examined the effect of ND after neurons have been seeded and developed, which is the state of the damaged neurons to be treated.

It has been demonstrated that microtubule stabilization with taxol can induce axon regeneration and improve functional outcome^{20,21}. We have previously shown that taxol can be covalently linked to NDs and this ND-taxol blocked the tumor growth *in vivo*⁸. These observations suggested the possibility of using ND to deliver taxol into injured nervous system in order to promote nerve regeneration. We selected FND in this study for its fluorescent property and high photostability. To minimize diffusion once FND has been injected into the nervous system, we decided to use FND with the size of 100 nm.



We first examined the biocompatibility of FND *in vitro* and discovered that FND did not induce cytotoxicity in CNS or PNS neurons. Intracranial injection of FND into the hippocampi of live rats did not cause gross behavioral differences compared to saline-injected rats. In addition, we demonstrated that FND could be internalized by neurons *in vitro* using flow cytometry and confocal microscopy. Surprisingly, we also discovered that FND caused a dosage-dependent decrease on neurite length in both CNS and PNS neurons *in vitro*. Finally, we performed live cell imaging on neurons treated with FND *in vitro* and found that the neurite length reduction effect was most likely the result of FND aggregates serving as spatial hindrance instead of as growth cone poison.

Results

Fluorescence nanodiamonds did not induce cytotoxicity in CNS or PNS neurons. To test whether FNDs exhibit any cytotoxic effect on neurons, we utilized two primary neuron cultures: mouse hippocampal neurons (represent CNS neurons) and mouse dorsal root ganglion (DRG) neurons (represent PNS neurons). Both neurons were isolated from embryonic mouse pups and seeded into optical bottom 96-well plates to facilitate image acquisition and analysis. Various dosages of FNDs (1, 5, 10, 25, 50, 100, 250 $\mu\text{g}/\text{mL}$) were then applied to the hippocampal neurons DRG neurons (Figure 1). After fixation, neurons were immunofluorescence stained with antibody against neuron-specific β -III-tubulin and the DNA stain DAPI. Images of hippocampal or DRG neurons were acquired using an automated fluorescence microscope. We quantified the number of neurons remain attached to the culture surface. This is a reliable indicator of viable neurons, because toxin-induced cell death caused neurons to detach from the culture surface. The neuron morphology quantification software Neurphology²² was used to

quantify the number of neurons in hippocampal and DRG neuron cultures after FND treatment. We did not detect any significant change in hippocampal or DRG neuron number under various FND dosages (Figure 2). In addition, we analyzed the fragmentation of the nuclear DNA after FND treatment. This is because cells undergoing apoptosis often exhibit fragmented nuclear DNA²³. The circularity of the nuclear DNA was measured in FND treated neurons to deduce the morphology of the nuclear fragmentation. Nuclear DNA in healthy cells displays high circularity (>0.7), whereas those undergoing apoptosis display low circularity (<0.5). None of the FND dosage we examined altered the circularity of the nuclear DNA in dissociated hippocampal neurons (Figure 3). Finally, we examined the level of activated caspase-3 in dissociated hippocampal neurons after FND treatment. Caspase-3 exists as inactive a proenzyme that needs to undergo proteolytic cleavage to generate the activated caspase-3, and this is a well-known apoptotic marker in various cell types including neurons^{24–26}. None of the FND dosages we examined significantly increased the level of activated caspase-3 in hippocampal neurons (Figure S1). Taken together, these results indicate that FNDs did not induce cytotoxicity at concentration up to 250 $\mu\text{g}/\text{mL}$.

Intracranial injection of fluorescence nanodiamonds did not alter gross animal behavior. To further examine the effect of FNDs on the nerves system *in vivo*, we intracranially injected 10 μL of FNDs at a concentration of 100 $\mu\text{g}/\text{mL}$ into the hippocampi of post-weaned juvenile rats. After the injection, the body weight, fodder and water consumption were assessed on a daily basis for one week. There were no significant differences in the daily changes of body weight or the daily consumption of fodder or water between FND- and saline-injected rats (Figure 4A–C). We also performed a behavioral test to determine whether there were more subtle effects of FNDs on the hippocampus. The novel object recognition test (NORT),

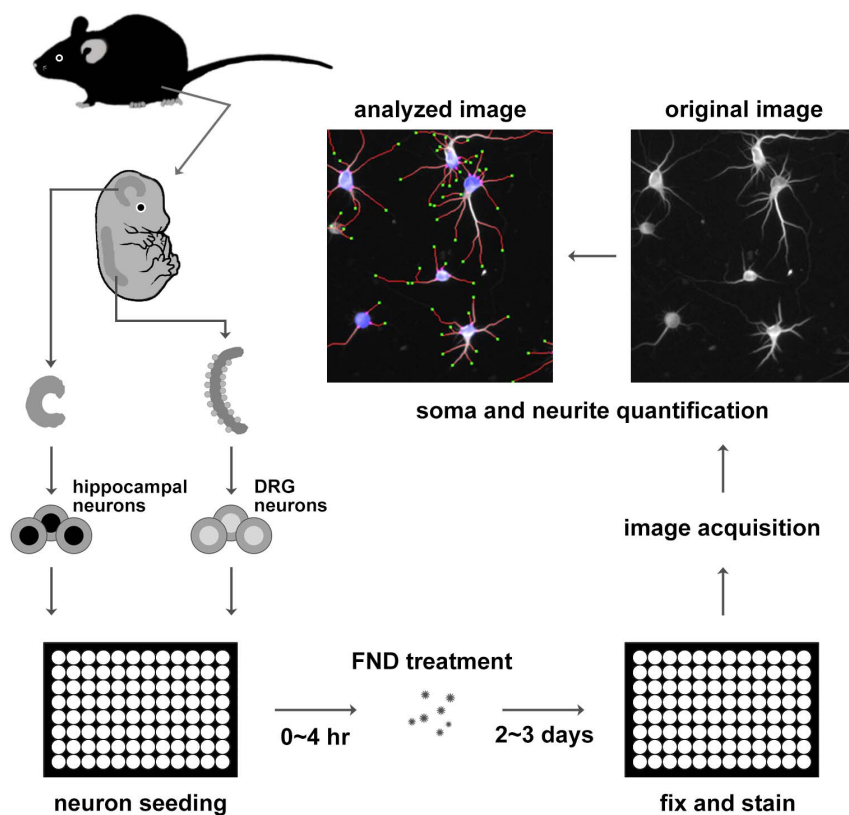


Figure 1 | Schematic diagram of dissociated primary neurons preparation, fluorescent nanodiamond treatment, and imaging procedure. Primary neurons from mouse hippocampi and the dorsal root ganglia were isolated from embryonic mice, dissociated with protease, and seeded into 96-well plates. Dissociated neurons were treated with FNDs for 2 ~ 3 days, fixed, and immunofluorescence stained with antibody against neuron-specific β -III-tubulin. Automated image acquisition and analysis were performed on stained neurons.

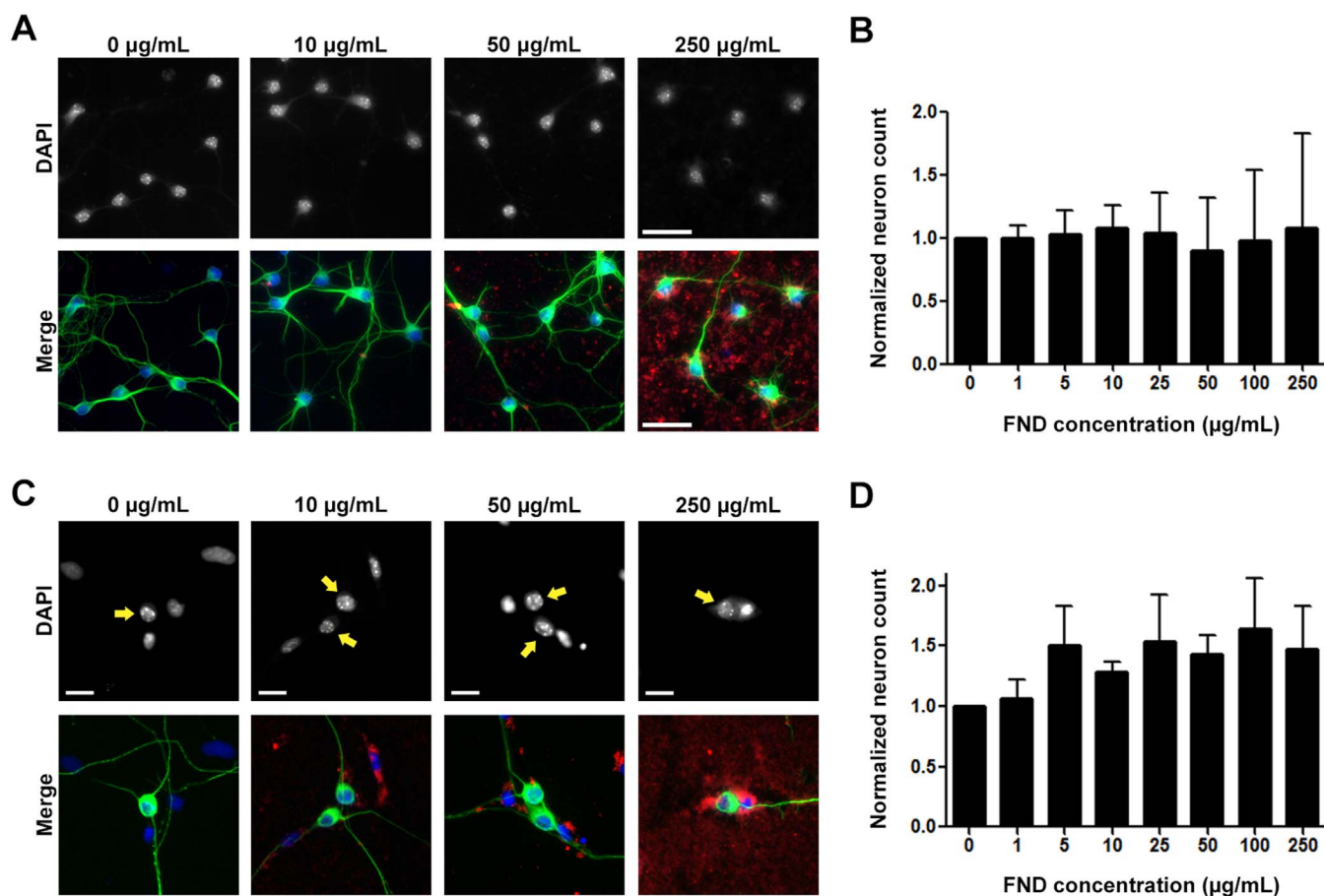


Figure 2 | Fluorescent nanodiamonds did not cause cytotoxicity in dissociated hippocampal or dorsal root ganglion neuron cultures. (A) Images of dissociated hippocampal neurons treated with various concentrations of FNDs 4 hours after seeding and incubated for 3 days *in vitro*. Images on the top row show DAPI-stained nuclei, merged images on the bottom row show FND (red), neuron-specific β -III-tubulin (green), and DAPI-stained nuclei (blue). Scale bars represent 50 μ m. (B) Quantification of neuron number per image field of FND treated hippocampal neurons. (C) Images of dissociated DRG neurons treated with various concentrations of FNDs after seeding and incubated for 2 days *in vitro*. Arrows point to the nuclei of DRG neurons. Scale bars represent 20 μ m. (D) Quantification of neuron number per image field of FND treated DRG neurons. All quantification data were obtained from 3 independent repeats and normalized to the group without FND. No statistically significant difference between control group and FND-treated groups can be detected. $p > 0.05$, by one-way ANOVA. Both bar graphs are expressed as mean \pm SEM.

developed by Ennaceur and Delacour²⁷, is based on the natural preference of rats to explore novel objects more than familiar ones. It has been shown that drugs which can damage the hippocampus lowered the discriminating index of NORT^{28,29}. Therefore, we used NORT to assess the effects of FNDs on hippocampal neurons in behaving animals. Neither the procedure of intracranial injection nor the injection of FNDs to the hippocampus altered the discriminating index of NORT (Figure 4D). These results suggested that FNDs didn't interfere with the general function of the hippocampus in live animals.

Fluorescence nanodiamonds can be internalized by neurons. It has been well documented that FNDs can be taken up by cancer cells^{9,30}. And it has recently been documented that FNDs can also be taken up by neurons derived from embryonal carcinoma cells *in vitro*¹⁷. To confirm whether FNDs can be internalized by primary neurons, we treated dissociated mouse cortical neurons with 0, 50, 250 μ g/mL of FNDs for 3 days and examined using flow cytometry (Figure 5). The red fluorescence intensity from FNDs was excited with a 488 nm laser and the emission was collected at 650 ~ 750 nm wavelength range with flow cytometry. We detected a FND dosage-dependent increase in FND fluorescence signal, suggesting FNDs remain associated with dissociated neurons after they were released from the culture surface. However, flow cytometry cannot distinguish

whether FND localized on the surface or the inside of neurons. Therefore, confocal microscopy was utilized to determine whether FND was indeed internalized by neurons. We treated dissociated mouse cortical neurons with 20 μ g/mL of FNDs for 2 days, fixed, and stained with concanavalin-A and DAPI to detect plasma membrane and nuclear DNA. Clusters of FNDs can be detected inside the cell bodies of the cortical neurons (Figure 6). Interestingly, internalized FND clusters were surrounded by concanavalin-A-containing organelles (Figure 6C–E). To assure the red fluorescence came from FNDs, we repeated scanned the soma region in an attempt to photobleach all fluorophores except the unbleachable FNDs. Indeed, the only remaining fluorescence after the photobleaching process was the red emission from FNDs (data not shown). These results demonstrated that FNDs can be internalized by neurons, and internalized FNDs tend to aggregated together inside membrane-surrounded organelles.

Fluorescence nanodiamonds affected neuronal morphogenesis in CNS and PNS neurons. Even though FNDs did not have any cytotoxic effect for neurons *in vitro* and *in vivo*, there remains a possibility that they can interfere with normal neuronal morphogenesis, a process requires intricate interaction between neurons and their extracellular environment. One of the most prominent morphological features of neurons is the elongated

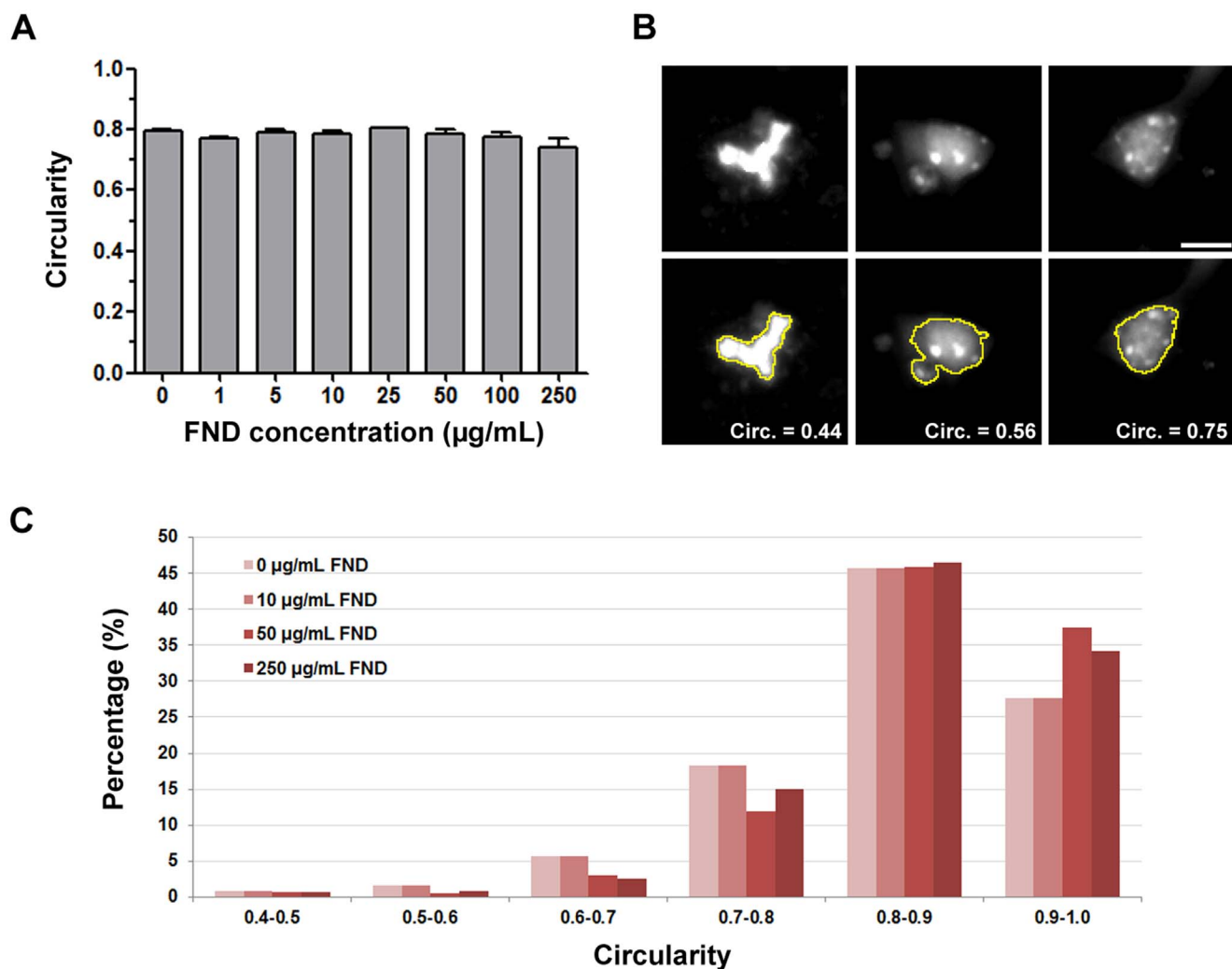


Figure 3 | Fluorescent nanodiamonds did not induce apoptosis in dissociated hippocampal neuron cultures. (A) Quantification of nucleus circularity in hippocampal neurons treated with various concentrations of FND. All quantification data were obtained from 3 independent repeats. No statistically significant difference between control group and FND-treated groups can be detected. $p > 0.05$, by one-way ANOVA. The bar graph is expressed as mean \pm SEM. (B) Representative images of cell nuclei with various circularity. Images on the top row show DAPI-stained nucleus and images on the bottom row show DAPI stained nucleus overlaid with ImageJ detected nuclear outline. The scale bar represents 10 μ m. (C) Histogram of nucleus circularity in hippocampal neurons treated with various concentrations of FND.

neurites. We therefore examined the effect of FNDs on neurite length. Various dosages of FND (1, 5, 10, 25, 50, 100, 250 μ g/mL) were applied to the cultured neurons (hippocampal neurons for 3 days and DRG neurons for 2 days). Due to the excessive growth of axons after 48 hours (which interfered with our image analysis), DRG neurons were treated with FNDs for only 2 days. After fixation and immunofluorescence staining, images of neurons were acquired using the automated fluorescence microscopy and the neurite length of hippocampal or DRG neurons was quantified using NeurphologyJ²² (Figure 1). Surprisingly, FNDs provoked a dosage-dependent reduction in neurite length in both CNS hippocampal neurons (Figure 7) and PNS DRG neurons (Figure 8). Furthermore, we discovered a striking morphological alteration in DRG neurons under high dosage FND treatment (100 μ g/mL and above). Almost all DRG neurons generated numerous terminal branches under this condition (Figure 8A). To better understand the neurite length reduction effect of FNDs, we performed live cell imaging on DRG neurons after treatment with low dosage of FND (1 μ g/mL) for 24 hours. We observed that the advancing growth cone of the DRG neuron stopped and retracted whenever it encountered FND clusters (Figure 9). However, this

growth cone remained motile and regrew after selecting a different advancing route (Figure 9 and supplemental movies). This result suggested that the reduction of neurite length was due to the FND acting as a spatial hindrance of the advancing neuronal growth cone instead of acting as a poison that compromised the motility of the growth cone.

Discussion

Consistent with previous researches^{15–17,31}, we did not observe any cytotoxic effect of FND on primary CNS or PNS neurons. Furthermore, intracranial injection of FND into the hippocampus of the rat did not alter the animal behavior. We did notice a slight increase of GFAP-positive astrocytes in FND-injected hippocampus compared to saline-injected hippocampus (data not shown). However, the sample size of this observation was rather small and requires further examination. While FND uptake has been observed in neurons derived from embryonal carcinoma cells¹⁷, neurons have very different membrane protein composition and whether other types of neurons can uptake FND remained unclear. Here we demonstrated that FNDs could be internalized by primary cortical neurons *in vitro*. The fact that FNDs can be internalized by neurons

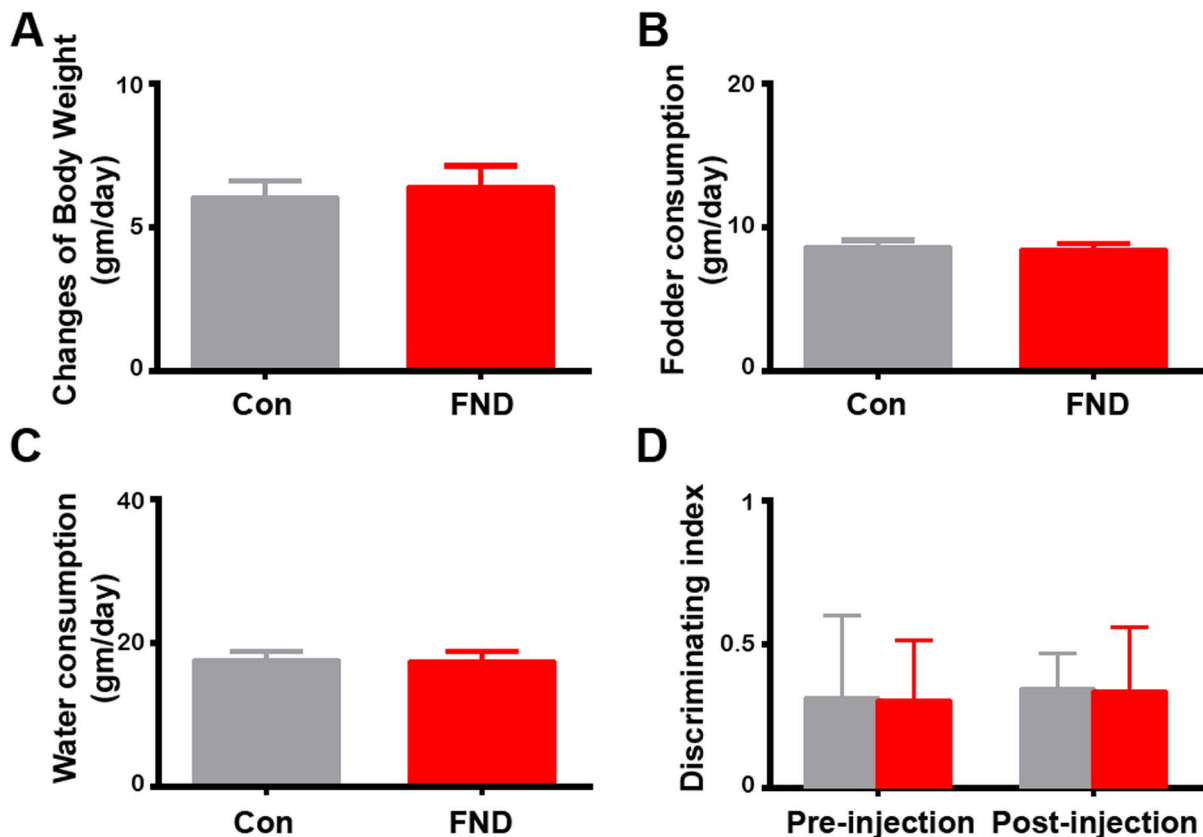


Figure 4 | Intracranial injection of fluorescence nanodiamonds did not alter body weight change, fodder and water consumptions, nor the performance of novel object recognition test. Quantification of daily changes of body weight (A), fodder (B), and water (C) consumption per day in control (saline-injected, $n=4$) and FND-injected ($n=4$) rats. No statistically significant difference between control and FND-treated groups can be detected. $p > 0.05$, by Wilcoxon sign rank test. (D) Quantification of discriminating index of NORT in control ($n=4$) and FND-injected ($n=4$) rats before and after intracranial injection. No statistically significant difference between control and FND-injected groups before and after intracranial injection can be detected. No interactions between the intracranial injections and FND treatments. $p > 0.05$, by two-way ANOVA repeated measurements. All bar graphs are expressed as mean \pm SEM.

hints at their applications as neurite tracer. We do not yet know whether internalized FNDs possess anterograde and/or retrograde motility.

We observed a dosage-dependent decrease of neurite length in both CNS and PNS neuron cultures in this study. However, a recently

research showed that ND-coated surface enhanced neurite outgrowth in CNS neuron culture¹⁶. These seemingly contradicting results may be explained by the particle size of the NDs used and the attachment of NDs to the culture surface. While FNDs utilized in our study have an average size of 114.7 nm, the previous study used

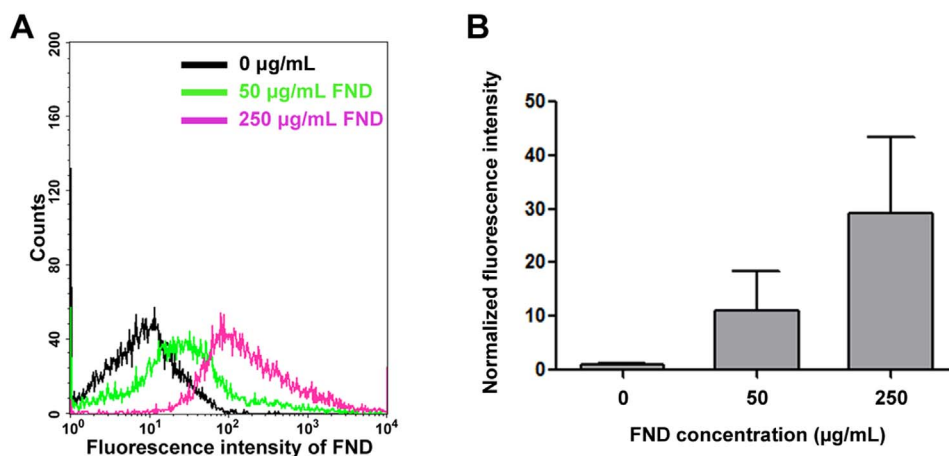


Figure 5 | The uptake ability of fluorescent nanodiamonds in dissociated neurons by flow cytometry analysis. (A) Dissociated mouse cortical neurons treated with 0, 50, or 250 $\mu\text{g/mL}$ FND for 3 days. FNDs were excited by with the 488 nm wavelength light, and the emitted light was collect in >650 nm wavelength range. (B) The fluorescence intensity of FND was quantified from a minimum of 10,000 cells using CellQuest software. Data were collected from 3 independent experiments, and the bar graph is expressed as mean \pm SEM.

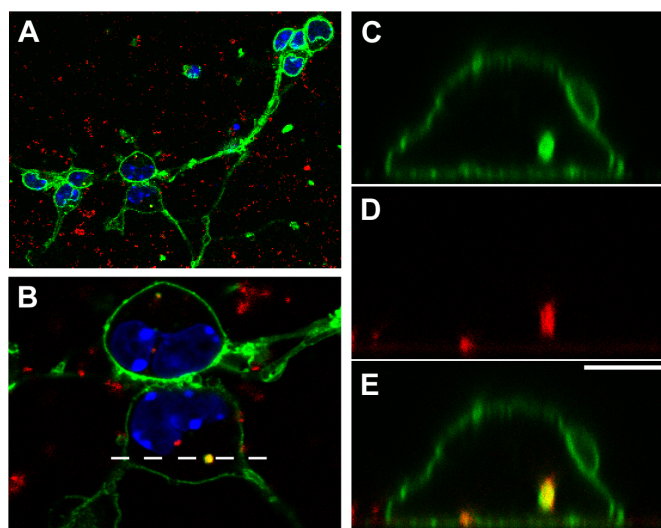


Figure 6 | Fluorescent nanodiamonds can be internalized into dissociated neurons. Confocal image of dissociated mouse cortical neurons cultured in the presence of 20 $\mu\text{g}/\text{mL}$ FND for 2 days, fixed, and stained with Alexa Fluor 488-conjugated concanavalin-A and DAPI. (A) Image of the entire field. FNDs are shown in red, concanavalin-A-stained membrane in green, and DAPI-stained nuclei in blue. (B) Zoom-in image of the 2 cortical neuron cell bodies in the boxed area of panel A. (C) XZ section of the concanavalin-A channel. (D) XZ section of the FND channel. (E) XZ section of the merged image. The dotted line in panel B indicates the location of the XZ sectioning shown in panel C–E. Scale bar in panel E represents 5 μm .

NDs with the size ranging from 20 nm to 35 nm¹⁶. The same research also showed that the particle size of the ND is negatively correlated with the neurite length, with the smallest ND particles promoting the best neurite outgrowth¹⁶. FNDs utilized in our study were not pre-coated on the culture surface and might form even larger aggregates. It is therefore possible that when the particle size exceeds a certain threshold, the neurite promoting effect may switch to a neurite inhibitory effect. Another origin of the discrepancy may come from the attachment of ND to the culture surface. FNDs we applied to our neuronal cultures were not pre-attached on the culture surface, but Edgington *et al.* used various approaches to attach their NDs to the surface. Although we did not observe prominent movements for large FND aggregates (Figure 9 and supplemental movies), it is a possibility that smaller FND particles invisible to phase contrast microscopy were moving on the culture surface and compromising neurite extension.

Interestingly, a recent paper showed that titanium dioxide, silicon dioxide, and hydroxyapatite nanoparticles could destabilize the microtubule cytoskeleton and induce focal adhesion remodeling³². We do not believe FNDs caused microtubule disruption as microtubule filaments can still be observed in neurons treated with 250 $\mu\text{g}/\text{mL}$ of FNDs (data not shown). Furthermore, our live cell imaging experiment showed that axon extension, a process that requires intact microtubule cytoskeleton, was not impaired in FND-treated DRG neurons.

In addition to the reduced neurite length, we also observed a drastic alteration of neurite morphology in DRG neurons under high dosage of FND (Figure 8A). Numerous terminal branches can be seen reminiscent of the synaptic terminals of unmyelinated DRG axons observed *in vivo*³³. Whether these terminal branches had really developed into synapses in our high-dosage FND cultures reminds to be tested. Nonetheless, the drastic morphological changes caution any ND application involves actively growing neurites (e.g. nerve regeneration). It is also worth noting that some nanomaterials have

been shown to disrupt the homophilic interaction of VE-cadherin at the adherens junction of the endothelial cells³⁴. Whether FNDs affect the synaptic junction between neurons remains to be tested.

Methods

FND preparation. NDs with an average size of 100 nm were purchased from Element Six (Micron + MDA, Element Six, Ireland). ND powders were radiation-damaged by using either a 40-keV He⁺ beam at a dose of $\sim 1 \times 10^{14}$ ions/cm² or a 3-MeV H⁺ beam at a dose of $\sim 1 \times 10^{16}$ ions/cm² to create the optimum amount of vacancies in the diamond crystal lattice, as previously described¹⁰. ND particles were subsequently annealed in vacuum at 800 °C for 2 hours to form FND. The nitrogen-vacancy-containing particles were extensively rinsed in distilled deionized water and stored at room temperature prior to use. The particle size and morphology of FNDs were examined by a scanning electron microscope (S6700, JEOL, Japan) (Figure S2). The average size of FNDs was around 114.7 ± 8.4 nm when analyzed by dynamic light scattering (BI-200SM, Brookhaven Instruments, Holtsville, NY) (Figure S3). We also observed that our FNDs carried negative charge around -20.65 ± 1.63 mV as determined by zeta potential analysis (ZetaPALS, Brookhaven Instruments, Holtsville, NY).

Primary neuron cultures. All experimental procedures were approved by the Institutional Animal Care and Use Committee (IACUC) of National Chiao Tung University (NCTU) and in accordance with the Guide for the Care and Use of Laboratory Animals.

Hippocampal neurons from E18 mouse embryos (C57BL/6) were prepared as described³⁵. Dissociated hippocampal neurons were seeded into poly-L-lysine-coated 96-well optical bottom plates at the density of 2×10^4 cells per well in 200 μL serum-containing neuronal plating medium (minimum essential medium supplemented with 5% fetal bovine serum, 0.6% D-glucose, and 2 mM L-glutamine; Life Technologies, Carlsbad, CA). The serum-containing medium was replaced with 100 μL serum-free neuronal maintenance medium (neurobasal medium with B27 supplement and 0.5 mM L-glutamine; Life Technologies) 3 hours after seeding. 100 μL of $2 \times$ FND-containing serum-free neuronal maintenance medium was added 4 hours after seeding. Neurons were treated with 1, 5, 10, 25, 50, 100, or 250 $\mu\text{g}/\text{mL}$ of FND. FND stock solution was vortexed for 30 seconds and sonicated for 30 mins before diluted in serum-free neuronal maintenance medium to minimize aggregation.

DRG neurons from E14 mouse embryos (C57BL/6) were prepared as described³⁶. Dissociated DRG neurons were seeded into poly-L-lysine- and laminin-coated 96-well optical bottom plates at the density of 3×10^3 cells per well in serum-free DRG growth medium (neurobasal medium with 25 ng/mL NGF, B27 supplement, 2 mM L-glutamine, Life Technologies). Neurons were treated with 1, 5, 10, 25, 50, 100, or 250 $\mu\text{g}/\text{mL}$ of FND at the time of seeding. FND stock solution was vortexed for 30 seconds and sonicated for 30 mins before diluted in serum-free DRG growth medium to minimize aggregation.

Immunofluorescence staining and microscopy. Hippocampal and DRG neurons were fixed with 3.7% formaldehyde in 1xPBS at 37 °C for 15 mins and 30 mins, respectively. Fixed neurons were permeabilized with 0.25% triton X-100 for 5 mins at room temperature, and blocked for 30 mins at 37 °C with 10% BSA. Neurons were incubated for 1 hour at 37 °C with primary antibodies (TUJ1, 1 : 4000, Covance; cleaved caspase-3 antibody, 1 : 400, Cell Signaling) in 2% BSA. Alexa Fluor 488-labeled secondary antibodies (1 : 1000, Life Technologies) were incubated for 1 hour at 37 °C in the dark. Fluorescence images were acquired with a Nikon Eclipse-Ti inverted microscope equipped with a Photometrics Coolsnap HQ² CCD camera. A 10×0.45 N.A. Plan Apochromat objective lens and the Nikon NIS-Element imaging software were used to automatically acquire fluorescence images for neuronal morphology quantification. A 20×0.75 N.A. Plan Apochromat objective lens was used to automatically acquire fluorescence images for activated caspase-3 quantification.

Live cell imaging was performed on the same Nikon microscope equipped with a Tokai Hit TIZHB live cell chamber. Time-lapse series were acquired using a 20×0.45 N.A. Ph1 Plan Fluor objective. Time-lapse series were acquired at 5 mins intervals. Dissociated DRG neurons were cultured with or without 1 $\mu\text{g}/\text{mL}$ FNDs in a poly-L-lysine- and laminin-coated 12-well plate for 18 hours. Live cell imaging was conducted for the subsequent 22 hours.

For confocal microscopy of dissociated neurons, 5×10^5 mouse cortical neurons were seeded into a 35 mm optical bottomed dish (μ -dish, ibidi, Germany) in serum-containing neuronal plating medium. The serum-containing medium was replaced by freshly made serum-free neurobasal medium containing 20 $\mu\text{g}/\text{mL}$ of FND 4 hours afterwards. Neurons were fixed 2 days after seeding with 3.7% formaldehyde in 1xPBS for 15 mins at 37 °C. After washing with 1xPBS three times, neurons were incubated with Alexa Fluor 488-labeled concanavalin-A (50 $\mu\text{g}/\text{mL}$, Life Technologies) and DAPI (5 $\mu\text{g}/\text{mL}$, Life Technologies) for 1 hour at 37 °C. FND particles were excited with wavelength centered at 580 nm and the emission was collected in the wavelength range of 610 ~ 750 nm using a Leica TCS-SP5-X microscopy system.

Cleaved caspase-3 quantification. Dissociated hippocampal neurons treated with FNDs were fixed and immunofluorescence stained as previously described. DAPI stained images were used to identify the location of the nuclei, and the signal of the

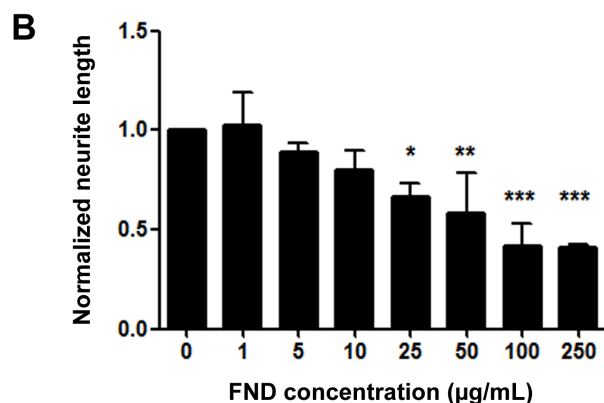
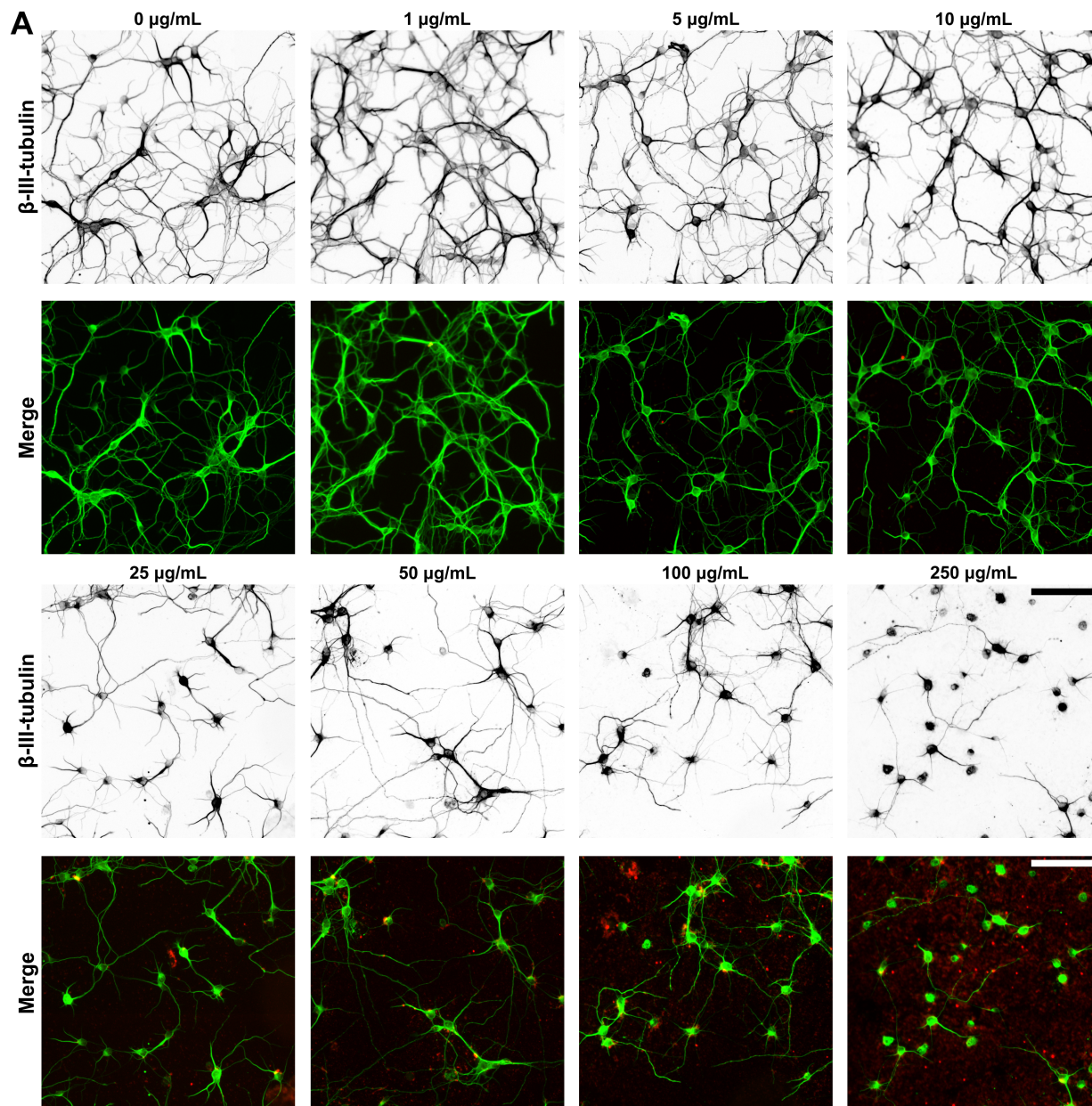


Figure 7 | Fluorescent nanodiamonds reduced neurite outgrowth in a dosage-dependent manner in dissociated hippocampal neurons. (A) Images of dissociated hippocampal neurons treated with various concentrations of FNDs 4 hours after seeding and incubated for 3 days *in vitro*. Images on the top row show β -III-tubulin staining (inverted to enhance visibility), merged images on the bottom row show FND (red) and β -III-tubulin staining (green). Scale bars represent 100 μ m. (B) Quantification of total neurite length per neuron in FND treated hippocampal neurons. All quantification data were obtained from 3 independent repeats and normalized to the group without FND. * $p < 0.05$, ** $p < 0.01$, *** $p < 0.001$ one-way ANOVA followed by Dunnett's post-hoc analysis against the control group (0 μ g/mL FND). The bar graph is expressed as mean \pm SEM.

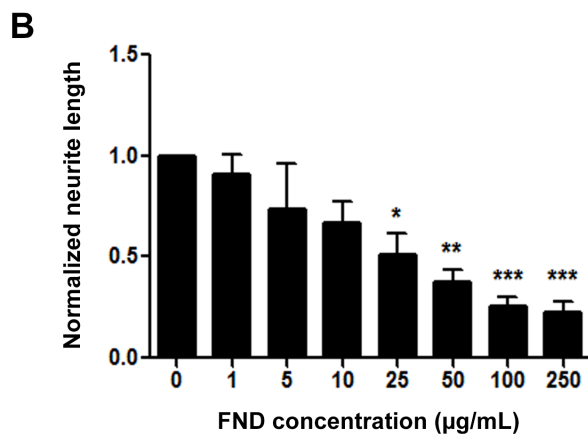
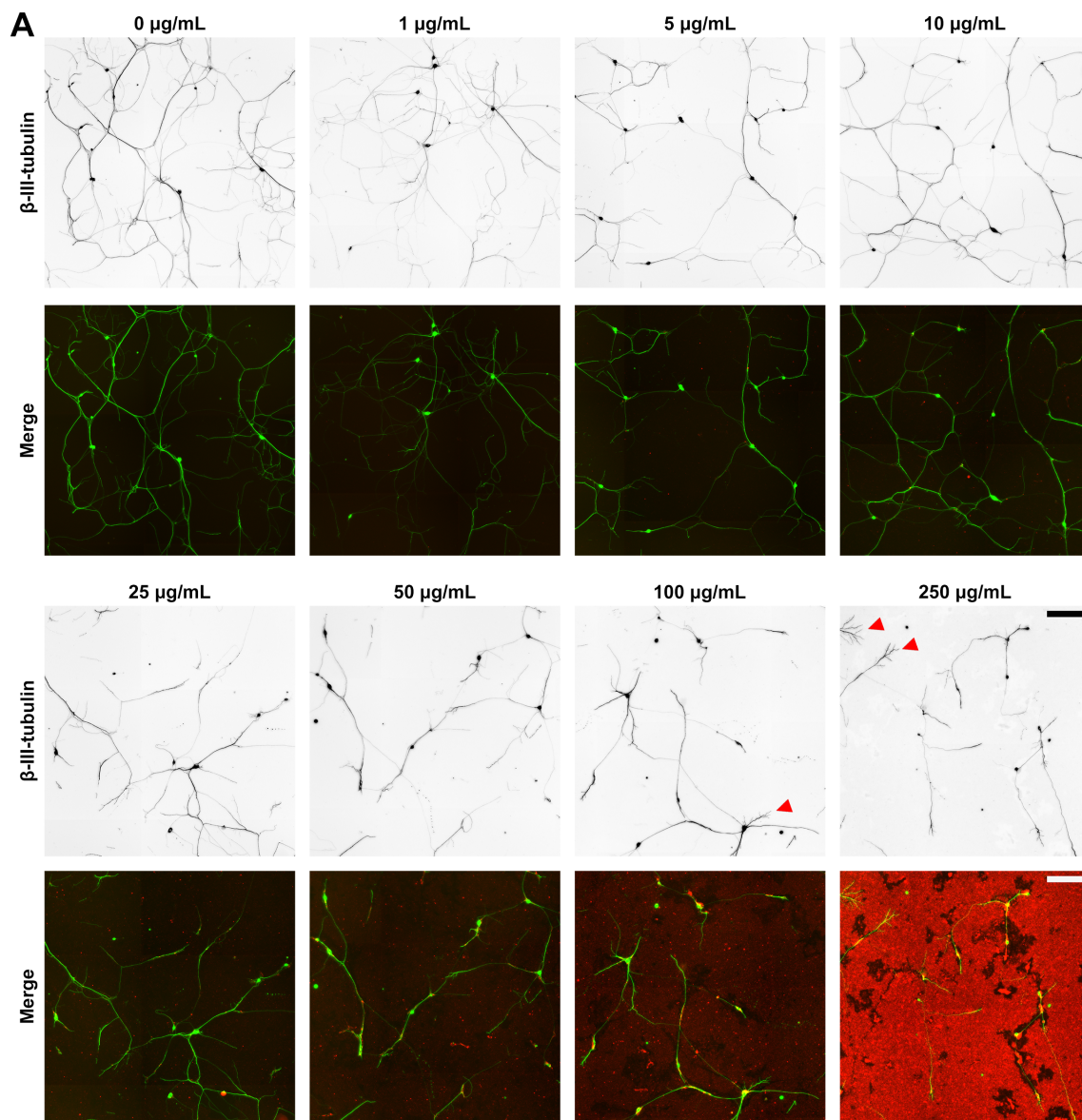


Figure 8 | Fluorescent nanodiamonds reduced neurite outgrowth in a dosage-dependent manner in dissociated dorsal root ganglion neurons. (A) Images of dissociated DRG neurons treated with various concentrations of FNDs after seeding and incubated for 2 days *in vitro*. Images on the top row show β -III-tubulin staining (inverted to enhance visibility), merged images on the bottom row show FND (red) and β -III-tubulin staining (green). Red arrow heads point to neurite terminal with numerous branches. Scale bars represent 200 μ m. (B) Quantification of total neurite length per neuron in FND treated DRG neurons. All quantification data were obtained from 3 independent repeats and normalized to the group without FND. * $p < 0.05$, ** $p < 0.01$, *** $p < 0.001$ one-way ANOVA followed by Dunnett's post-hoc analysis against the control group (0 μ g/mL FND). The bar graph is expressed as mean \pm SEM.

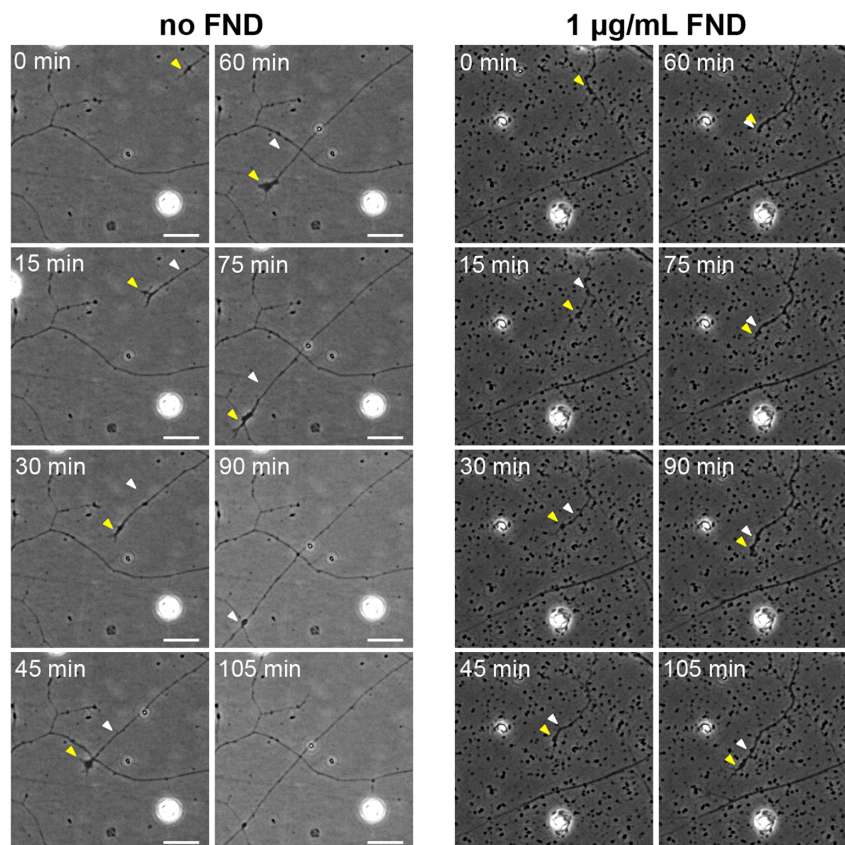


Figure 9 | Fluorescent nanodiamond clusters acted as spatial hindrance on advancing neuronal growth cones. The time-lapse phase contrast image sequences showing the advancing growth cones of DRG neurons under no (left panels) or 1 $\mu\text{g}/\text{mL}$ of FND (right panels) treatment for 1 day. The yellow arrowhead points to the growth cone for the current time, and the white arrowhead points to the growth cone at the previous time. All images have the same magnification and all scale bars represent 20 μm .

activated (cleaved) caspase-3 inside the nuclei was quantified using ImageJ. To eliminate the spectral bleed through of FND into the caspase-3 channel, signal before immunofluorescence staining was subtracted from the final caspase-3 signal.

Intracranial injection. All experimental procedures were approved by the IACUC of NCTU and in accordance with the Guide for the Care and Use of Laboratory Animals. A total of 8 post-weaned juvenile rats (3 weeks old, 40–50 g, from BioLASCO, Taiwan) were used in this experiment. Each pair of control and experimental rats was selected from the same litter to minimize genetic variations. Both control and experimental rats were anesthetized with isoflurane (5% for induction and 2% for maintenance) and mounted on the standard stereotaxic instrument (Stoelting, Wood Dale, IL). A small hole was drilled according to landmarks in Paxinos and Watson's standard brain atlas³⁷. 10 μL of FNDs (100 $\mu\text{g}/\text{mL}$) containing saline were injected into the experimental group hippocampi with a 31-gauge injection cannula that was connected to a 10 μL microsyringe (Hamilton, Reno, NV) (Figure S4A). The solution was infused over a 10 min period and the needle was left in hippocampus for 2 min after the end of infusion. Control rats were injected with 10 μL saline. After the injection cannula was removed, Spongostan film (Ferrosan Medical Devices, Denmark) and bone wax (WPI Inc., Sarasota, FL) were covered on the opening of the skull and the resected skins were closed with fine suture (5/0; UNIK, Taiwan). After recovered from the anesthesia, rats were housed in individual chambers. The wounds, body weight, fodder and water consumptions were assessed on a daily basis. The daily changes of body weight, fodder and water consumptions were averaged and compared between experimental and control groups.

The novel object recognition test (NORT). The experimental environment (78 cm \times 56 cm \times 46 cm) was surrounded by white walls and the floor was covered with wood bedding. Objects were placed at the symmetrical positions 26 cm from the left or right sides, and 28 cm from the upper and lower sides of the box. At the end of each session, the 70% ethanol was used to clean the objects and box to remove any olfactory cues on the objects and in the box. To minimize the bias for the specific location, the familiar and non-familiar objects were randomly placed at the left or right position. To habituate to the perimetal environment, rats were placed in the box and allowed for exploration for 15 min an hour before the behavioral measurement. NORT consisted of the training and testing sessions and they were separated by a retention interval of 1 hour (Figure S4B). NORT were conducted 1 week before and after the intracranial FNDs injection. During the training session, rats were placed in the box at

the center of two identical objects and allowed to explore for 10 min. At the end of the training session, the rats were return to the home cage and the two objects and the whole box were cleaned with 70% ethanol. After the retention interval, one familiar object was replaced by a novel object. In the testing session, rats were return to the box and exposed to the objects for 10 min. Both the training and testing session were recorded by a digital video camera and analyzed. The object exploration was defined as the rat pointing its nose to the object within 1 cm. The difference in time exploring the novel versus familiar objects normalized by the total exploring time for both objects in the testing session was the discriminating index (DI). The population data of DI was expressed as mean \pm SEM. The effects of intracranial injections of FNDs were assessed by the two-way ANOVA with repeated measurements.

Flow cytometry. Mouse cortical neuron cells were plated at a density of 5×10^6 cells in a 6-well plate coated with poly-L-lysine in serum-containing neuronal plating medium for 4 hours. The serum-containing medium was replaced by freshly made serum-free neurobasal medium containing various concentrations of FND 4 hours afterwards. Cells were treated with 0, 50, 250 $\mu\text{g}/\text{mL}$ FNDs and incubated for 72 hours. At the end of the incubation, cells were collected by treating with 0.25% trypsin at 37°C for 30 min, centrifuged at 1200 rpm, and fixed with ice-cold 70% ethanol overnight at -20°C . Thereafter, cells were centrifuged at 1200 rpm and cell pellets were re-dissolved with 1 mL 1xPBS. To avoid aggregation, fixed cells were filtered through a nylon membrane (BD Biosciences, San Jose, CA). A minimum of 1×10^4 cells in each samples were subjected to the fluorescence intensities analysis by CellQuest software in a flow cytometer (FACSCalibur, BD Biosciences). FNDs were analyzed by FL3 laser system (excitation: 488 nm; emission: 650 \sim 750 nm).

1. Mochalin, V. N., Shenderova, O., Ho, D. & Gogotsi, Y. The properties and applications of nanodiamonds. *Nat Nanotechnol* **7**, 11–23 (2012).
2. Krueger, A. New carbon materials: biological applications of functionalized nanodiamond materials. *Chemistry* **14**, 1382–1390 (2008).
3. Bouzigues, C., Gacoin, T. & Alexandrou, A. Biological applications of rare-earth based nanoparticles. *ACS Nano* **5**, 8488–8505 (2011).
4. Zhang, X. Q. *et al.* Multimodal nanodiamond drug delivery carriers for selective targeting, imaging, and enhanced chemotherapeutic efficacy. *Adv Mater* **23**, 4770–4775 (2011).



5. Chao, J. I. *et al.* Nanometer-sized diamond particle as a probe for biolabeling. *Biophys J* **93**, 2199–2208 (2007).
6. Chang, I. P., Hwang, K. C. & Chiang, C. S. Preparation of fluorescent magnetic nanodiamonds and cellular imaging. *J Am Chem Soc* **130**, 15476–15481 (2008).
7. Liu, K. K. *et al.* Alpha-bungarotoxin binding to target cell in a developing visual system by carboxylated nanodiamond. *Nanotechnology* **19**, 205102 (2008).
8. Liu, K. K. *et al.* Covalent linkage of nanodiamond-paclitaxel for drug delivery and cancer therapy. *Nanotechnology* **21**, 315106 (2010).
9. Lien, Z. Y. *et al.* Cancer cell labeling and tracking using fluorescent and magnetic nanodiamond. *Biomaterials* **33**, 6172–6185 (2012).
10. Chang, Y. R. *et al.* Mass production and dynamic imaging of fluorescent nanodiamonds. *Nat Nanotechnol* **3**, 284–288 (2008).
11. Vajjayanthimala, V. *et al.* The long-term stability and biocompatibility of fluorescent nanodiamond as an in vivo contrast agent. *Biomaterials* **33**, 7794–7802 (2012).
12. Yu, S. J., Kang, M. W., Chang, H. C., Chen, K. M. & Yu, Y. C. Bright fluorescent nanodiamonds: no photobleaching and low cytotoxicity. *J Am Chem Soc* **127**, 17604–17605 (2005).
13. Vajjayanthimala, V., Tzeng, Y. K., Chang, H. C. & Li, C. L. The biocompatibility of fluorescent nanodiamonds and their mechanism of cellular uptake. *Nanotechnology* **20**, 425103 (2009).
14. Xi, G. *et al.* Convection-enhanced delivery of nanodiamond drug delivery platforms for intracranial tumor treatment. *Nanomedicine* **10**, 381–391 (2014).
15. Thalhammer, A., Edgington, R. J., Cingolani, L. A., Schoepfer, R. & Jackman, R. B. The use of nanodiamond monolayer coatings to promote the formation of functional neuronal networks. *Biomaterials* **31**, 2097–2104 (2010).
16. Edgington, R. J. *et al.* Patterned neuronal networks using nanodiamonds and the effect of varying nanodiamond properties on neuronal adhesion and outgrowth. *J Neural Eng* **10**, 056022 (2013).
17. Hsu, T. C., Liu, K. K., Chang, H. C., Hwang, E. & Chao, J. I. Labeling of neuronal differentiation and neuron cells with biocompatible fluorescent nanodiamonds. *Sci Rep* **4**, 5004 (2014).
18. Kelly, S. *et al.* Patterned growth of neuronal cells on modified diamond-like carbon substrates. *Biomaterials* **29**, 2573–2580 (2008).
19. Specht, C. G., Williams, O. A., Jackman, R. B. & Schoepfer, R. Ordered growth of neurons on diamond. *Biomaterials* **25**, 4073–4078 (2004).
20. Sengottuvel, V., Leibinger, M., Pfreimer, M., Andreadaki, A. & Fischer, D. Taxol facilitates axon regeneration in the mature CNS. *J Neurosci* **31**, 2688–2699 (2011).
21. HELLAL, F. *et al.* Microtubule stabilization reduces scarring and causes axon regeneration after spinal cord injury. *Science* **331**, 928–931 (2011).
22. Ho, S. Y. *et al.* Neurphology): an automatic neuronal morphology quantification method and its application in pharmacological discovery. *BMC Bioinformatics* **12**, 230 (2011).
23. Cregan, S. P. *et al.* Apoptosis-inducing factor is involved in the regulation of caspase-independent neuronal cell death. *J Cell Biol* **158**, 507–517 (2002).
24. Nicholson, D. W. *et al.* Identification and inhibition of the ICE/CED-3 protease necessary for mammalian apoptosis. *Nature* **376**, 37–43 (1995).
25. Milligan, C. E. *et al.* Peptide inhibitors of the ICE protease family arrest programmed cell death of motoneurons in vivo and in vitro. *Neuron* **15**, 385–393 (1995).
26. Uetsuki, T. *et al.* Activation of neuronal caspase-3 by intracellular accumulation of wild-type Alzheimer amyloid precursor protein. *J Neurosci* **19**, 6955–6964 (1999).
27. Ennaceur, A. & Delacour, J. A new one-trial test for neurobiological studies of memory in rats. 1: Behavioral data. *Behav Brain Res* **31**, 47–59 (1988).
28. Akkerman, S. *et al.* Object recognition testing: methodological considerations on exploration and discrimination measures. *Behav Brain Res* **232**, 335–347 (2012).
29. Clark, R. E., Zola, S. M. & Squire, L. R. Impaired recognition memory in rats after damage to the hippocampus. *J Neurosci* **20**, 8853–8860 (2000).
30. Liu, K. K., Wang, C. C., Cheng, C. L. & Chao, J. I. Endocytic carboxylated nanodiamond for the labeling and tracking of cell division and differentiation in cancer and stem cells. *Biomaterials* **30**, 4249–4259 (2009).
31. Le, X. L. *et al.* Fluorescent diamond nanoparticle as a probe of intracellular traffic in primary neurons in culture. Colloidal Nanocrystals for Biomedical Applications VII Book Series: Proc of SPIE **8232**, 823203 (2012).
32. Tay, C. Y. *et al.* Nanoparticles strengthen intracellular tension and retard cellular migration. *Nano Lett* **14**, 83–88 (2014).
33. Sugiura, Y., Lee, C. L. & Perl, E. R. Central projections of identified, unmyelinated (C) afferent fibers innervating mammalian skin. *Science* **234**, 358–361 (1986).
34. Setyawati, M. I. *et al.* Titanium dioxide nanomaterials cause endothelial cell leakiness by disrupting the homophilic interaction of VE-cadherin. *Nat Commun* **4**, 1673 (2013).
35. Chen, W. S., Yueh, C. Y., Huang, Y. A. & Hwang, E. An inverted method for culturing dissociated mouse hippocampal neurons. *Neurosci Res* **70**, 118–123 (2011).
36. Huang, Y. A. *et al.* Microtubule-Associated Type II Protein Kinase A Is Important for Neurite Elongation. *PLoS One* **8**, e73890 (2013).
37. Paxinos, G. & Watson, C. *The rat brain in stereotaxic coordinates*, 6th ed. (Academic Press, Elsevier, Amsterdam, Boston, 2007).

Acknowledgments

This work was supported by grants from the National Science Council, Taiwan (NSC 102-2627-B-009-008, NSC 101-2311-B-009-004-MY3, and NSC 99-2311-B-009-003-MY3), Veterans General Hospitals University System of Taiwan Joint Research Program (VGHUST103-G5-4-3), and the Ministry of Education Aim for the Top University Plan. The authors wish to thank National Chiao Tung University Center for Advanced Instrumentation for providing the use of multiphoton and confocal microscope as well as total internal reflection fluorescence microscope.

Author contributions

Y.H., C.K., K.L., H.H., M.C. and C.S. conducted experiments. H.C. supplied materials and equipments. T.C., J.C. and E.H. designed experiments and wrote the manuscript. All authors discussed on the manuscript.

Additional information

Supplementary information accompanies this paper at <http://www.nature.com/scientificreports>

Competing financial interests: The authors declare no competing financial interests.

How to cite this article: Huang, Y.-A. *et al.* The effect of fluorescent nanodiamonds on neuronal survival and morphogenesis. *Sci. Rep.* **4**, 6919; DOI:10.1038/srep06919 (2014).



This work is licensed under a Creative Commons Attribution-NonCommercial-ShareAlike 4.0 International License. The images or other third party material in this article are included in the article's Creative Commons license, unless indicated otherwise in the credit line; if the material is not included under the Creative Commons license, users will need to obtain permission from the license holder in order to reproduce the material. To view a copy of this license, visit <http://creativecommons.org/licenses/by-nc-sa/4.0/>